

Electromagnetic Induction Imaging of concealed metallic objects by means of resonating circuits

R. Guilizzoni*^a, J.C. Watson^b, P.A. Bartlett^a and F. Renzoni^a

^aDepartment of Physics & Astronomy, University College London, Gower Street, London, WC1E 6BT, United Kingdom

^bNovel Detection Concepts, National Nuclear Security Programme, Atomic Weapons Establishment, Aldermaston, Reading, RG7 4PR, United Kingdom

ABSTRACT

An electromagnetic induction system, suitable for 2D imaging of metallic samples of different electrical conductivities, has been developed. The system is based on a parallel LCR circuit comprising a ferrite-cored coil (7.8 mm x 9.5 mm, $L=680 \mu\text{H}$ at 1 KHz), a variable resistor and capacitor. The working principle of the system is based on eddy current induction inside a metallic sample when this is introduced into the AC magnetic field created by the coil. The inductance of the LCR circuit is modified due to the presence of the sample, to an extent that depends on its conductivity. Such modification is known to increase when the system is operated at its resonant frequency. Characterizing different metals based on their values of conductivity is therefore possible by utilizing a suitable system operated at resonance. Both imaging and material characterization were demonstrated by means of the proposed electromagnetic induction technique. Furthermore, the choice of using a system with an adjustable resonant frequency made it possible to select resonances that allow magnetic-field penetration through conductive screens. Investigations on the possibility of imaging concealed metals by penetrating such shields have been carried out. A penetration depth of $\delta \sim 3$ mm through aluminium (Al) was achieved. This allowed concealed metallic samples- having conductivities ranging from 0.54 to 59.77 MSm^{-1} and hidden behind 1.5-mm-thick Al shields- to be imaged. Our results demonstrate that the presence of the concealed metallic objects can be revealed. The technique was thus shown to be a promising detection tool for security applications.

Keywords: Imaging, electromagnetic induction, eddy currents, material characterization, screening.

1. INTRODUCTION

Electromagnetic induction imaging (EII)¹⁻⁹ is a non-invasive and non-contact imaging technique that is based on the induction of eddy currents in a conductive sample placed in the AC magnetic field generated by a coil. Eddy current induction leads to a change in the magnetic field which can be exploited to produce conductivity maps of the sample. EII is largely exploited both for biomedical imaging applications¹⁻³ and in Non Destructive Evaluation (NDE) for crack detection during industrial inspections⁶⁻⁸. Recent work has been focused on the development of an EII detection system for applications in the field of National Nuclear Security⁹⁻¹⁰. A different approach has been undertaken by Deans *et al.*¹¹ and Marmugi *et al.*¹², who developed a radio-frequency atomic magnetometer showing promising results for crack detection as well as biomedical imaging. Recent work on EII systems has been directed towards the development of high-sensitivity detection and imaging methods for industrial applications. Among these, Q-detection sensors have been used for condition monitoring of steel reinforcing bars embedded in concrete⁷, and an inductance-capacitance resonance system has been proposed for detection of metallic wear debris in rotating and reciprocating machinery¹³⁻¹⁴.

Here, we demonstrate imaging of conductive samples shielded by conductive barriers, by means of a resonant LCR system. The impedance change occurring in such system due to the presence of a conductive sample changes the resonant frequency and Q-factor of the system and so opens a route to imaging and characterization. Previous work¹⁵ demonstrated a proof-of-principle technique for imaging of unshielded conductive samples, both magnetic and non-magnetic in nature. The proposed technique relies on eddy-current induction inside a conductive sample and exploits the inductance change occurring in the LCR detection system causing a variation in resonant frequency and Q-factor. Thus, position-resolved-measurements of the resonant frequency and Q-factor of the system allowed 2D imaging of unshielded samples having conductivity ranging from 0.54 MSm^{-1} (manganese, Mn) to 59.77 MSm^{-1} (copper, Cu).

*roberta.guilizzoni.13@ucl.ac.uk

Penetrating through metallic barriers is essential, in security applications, in order to identify ‘hidden’ conductive materials within the enclosure. Standard electromagnetic imaging systems do not in general allow imaging through conductive barriers due to limitations in the system’s resonant-field penetration depth; the inherent resonant frequency is typically too high and the subsequent skin depth smaller than the thickness of the barrier. Modification of the LCR circuit undertaken by introducing a tunable capacitor bank (decade box) allows the penetration depth through Al to reach a value of about 3mm as a result of a tunable resonant frequency. Implementation of our resonance-based EII system and the results obtained with both unshielded and shielded metallic samples are reported here.

2. MATERIALS AND METHOD

The experimental apparatus is shown in Figure 1. A ferrite-cored coil (part no. MCSCH895-681 KU, inductance value $L=(680\pm 10\%) \mu\text{H}$) is part of a parallel LCR circuit (Figure 1b) and works both as a coil inducing eddy-currents in samples and as a sensor detecting the changes in resonant frequency and Q-factor due to their presence (with respect to measurements made in air alone). Capacitor and resistor values can be selected by means of two decade boxes that allow capacitance and resistance values to be selected in the following ranges: C between 100 pF and 11.111 μF (100 pF steps); R between 1 Ω and 11.111 M Ω (1 Ω steps).

The LCR circuit in air, i.e. when no sample is present, resonates at a frequency f_r that depends on the values of its inductance L and capacitance C (Eq. 1):

$$f_r = \frac{1}{2\pi\sqrt{LC}} \quad (1)$$

The system’s resonant frequency is changed when a conductive sample is inductively coupled to it, as a direct consequence of the change in the system’s inductance. The new frequency f_r' will be given by:

$$f_r' = \frac{1}{2\pi\sqrt{L'C}} \quad (2)$$

Measurements of the resonant frequency shift should then allow identification of the conductive sample. Resultant shifts are dependent on the properties of the imaged sample. Moreover, the system Q-factor, Q , for the parallel LCR circuit

$$Q = R\sqrt{\frac{C}{L}} \quad (3)$$

changes as resonance changes, since this quantity is also dependent on the system’s inductance.

A proof-of-principle method has been developed that allows 2D imaging of conductive samples by means of position-resolved-measurements of the resonant frequency and Q-factor shifts occurring due to the presence of the samples. A procedure was developed that is based on scanning a given area by moving the conductive sample with the aid of a xy stage (Figure 1a), and plotting the measured values obtained at each position along the scanning area vs the corresponding x and y coordinates. Resonant frequency and Q-factor measurements were performed by means of an impedance analyzer (Wayne Kerr 6500 B). A Labview Virtual Instrument (VI) was created with the purpose of controlling the xy stage movements and performing measurements of the quantities of interest at each position defined by the nodes of the xy scanning area.

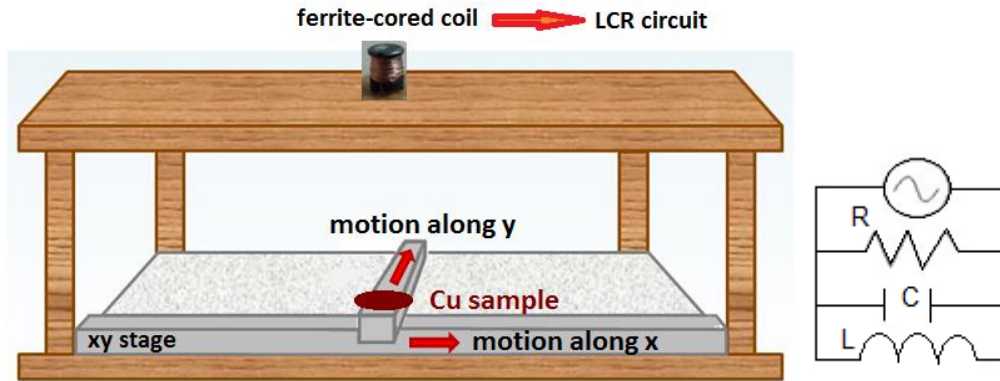


Figure 1. Sketch of the experimental apparatus, made up of a ferrite-cored coil connected to a capacitor and a resistor. A xy stage was used to move a metallic sample (such as the disk made of Cu shown above), thus allowing to perform a scan for imaging purpose. The apparatus is enclosed in a non-magnetic structure (made of wood), in order for the experiment to be electromagnetically isolated.

2.1 2D imaging of unshielded conductive samples

The experimental system was initially tested to see whether it could detect the presence of metallic samples placed at different values of lift-off (the vertical distance between sample and coil) between $l=0$ and $l=6$ cm. Metallic samples were used having conductivity values ranging from 0.54 MSm^{-1} (Mn) to 59.77 MSm^{-1} (Cu). The procedure undertaken had the aim of imaging each conductive sample. Position-resolved-measurements of the resonant frequency were performed in the absence of the sample to be imaged, along a xy scanning area (background readings). Resonant frequency values were then acquired at all nodes of the scanning area when the conductive sample was present: after each reading, the sample was moved onto the next position of the scan, and this was repeated until the whole scanning area was completed. Q-factor readings were also acquired in a similar fashion, by taking measurements first with no sample and then with the sample scanning the xy area. The values measured when the conductive sample was present were then normalized by dividing them by the background readings. Two matrices were thus obtained, which contained normalized values of the resonant frequency and the Q-factor respectively. The values in each matrix were plotted against the corresponding x and y coordinates and interpolated with a piecewise cubic function generated by Matlab. This resulted in two images being produced for each conductive sample, resulting from the resonant frequency and Q-factor acquisitions respectively.

2.2 LCR circuit optimization

Investigations were conducted with the purpose of optimizing the EII system used for 2D imaging of unshielded conductive samples. In particular, the aim of this study was to increase the Q-factor of the LCR circuit constituting the system, in order for it to acquire higher selectivity; indeed, higher values of Q mean sharper resonance peaks and thus imply the possibility to differentiate between similar resonances. This is essential in order to distinguish between materials of different nature that have similar values of conductivity and thus produce similar changes in the measured quantities (f_r and Q). Increasing the system resonant frequency selectivity is also important to enable imaging of low-conductivity samples, in which small amounts of eddy currents are induced, thus producing small changes in the measured quantities with respect to the background values. An experiment was conducted to this purpose, in which eight LCR circuits were built by selecting different combinations of resistance and capacitance, in order to vary the values of f_r and Q of the system, as predicted by equations (1) and (3). The LCR circuits that were built are labelled with numbers I-VIII in column 1 of Table 1, and the corresponding combinations of resistors and capacitors are reported in columns 2 and 3 of the same table. The relative changes Δf_r and ΔQ were determined for each of the eight LCR circuits, by means of equations (4) and (5):

$$\Delta f_r = \frac{f(\text{sample}) - f(\text{background})}{f(\text{background})} (\%) \quad (4)$$

$$\Delta Q = \frac{Q(\text{sample}) - Q(\text{background})}{Q(\text{background})} (\%) \quad (5)$$

In these equations, $f(\text{background})$ and $Q(\text{background})$ represent values measured for each LCR circuit when this was in air, and $f(\text{sample})$ and $Q(\text{sample})$ resulted from measurements taken with the same circuit after placing a $25 \times 25 \times 1 \text{ mm}^3$ Al sample under the coil, at a lift-off $l = (1.0 \pm 0.1) \text{ cm}$.

Table 1. Values of resistance (second column) and capacitance (third column) that were chosen to build eight different LCR circuits (labelled with numbers I-VIII reported in the first column of the Table).

LCR circuit number	Resistor value	C (μF , uncertainty $\pm 1\%$)
I	$(3.000 \pm 0.001) \text{ K}\Omega$	2.0
II	$(3.000 \pm 0.001) \text{ K}\Omega$	3.0
III	$(3.000 \pm 0.001) \text{ K}\Omega$	5.0
IV	$(1.000 \pm 0.001) \text{ M}\Omega$	2.0
V	$(1.000 \pm 0.001) \text{ M}\Omega$	3.0
VI	$(1.000 \pm 0.001) \text{ M}\Omega$	5.0
VII	$(2.000 \pm 0.001) \text{ M}\Omega$	0.5
VIII	$(4.000 \pm 0.001) \text{ M}\Omega$	1.0

This investigation aimed at finding the optimal LCR circuit, defined as the circuit which caused the greatest change in the measured quantities Δf_r and ΔQ .

2.3 2D imaging of shielded conductive samples

The main objective of this investigation was testing the ability of the EII system to penetrate through conductive barriers allowing 2D imaging of metallic objects concealed behind them. Eddy current flow is not uniformly distributed throughout the volume of the sample. In particular, current flow is stronger at the surface, and it decreases exponentially with the distance from the surface. The standard penetration depth (or skin depth, δ), defined as the depth within a conductor at which the eddy-current density decreases to a level of $\sim 37\%$ of its surface value, is given by:

$$\delta = \sqrt{\frac{1}{\sigma \mu f}}, \quad (6)$$

where σ is the sample's electrical conductivity, μ its magnetic permeability and f is the frequency at which the system is operated, which corresponds to its resonant frequency f_r (equation 1) in this experiment. The skin depth will have to be sufficiently high in order for penetration through conductive barriers to occur. According to formula (6), penetrating through these shields can be achieved by decreasing the system resonant frequency to an extent depending on the material's electromagnetic properties (identified by σ and μ). One way of decreasing f_r is to increase the capacitance, as is shown by the definition of resonant frequency contained in equation (1). Therefore, the capacitance of our EII system was set to the value $C = 11 \mu\text{F}$, in order for the skin depth through Al to be equal to 3.3 mm, and an imaging procedure similar to the one described in Section 2.1 (without acquisition of background readings) was applied to 2D imaging of conductive samples hidden behind 1.5-mm-thick Al shields.

3. RESULTS AND DISCUSSION

3.1 2D imaging of unshielded conductive samples

The main results of preliminary experiments aimed at imaging conductive samples in the unshielded configuration (see Sec. 2.1) are here reported. 2D plots of a 2-cm-diameter 2-mm thick Al disk are shown in Figure 2; these images were obtained by means of position-resolved-measurements of the resonant frequency (a) and Q-factor (b).

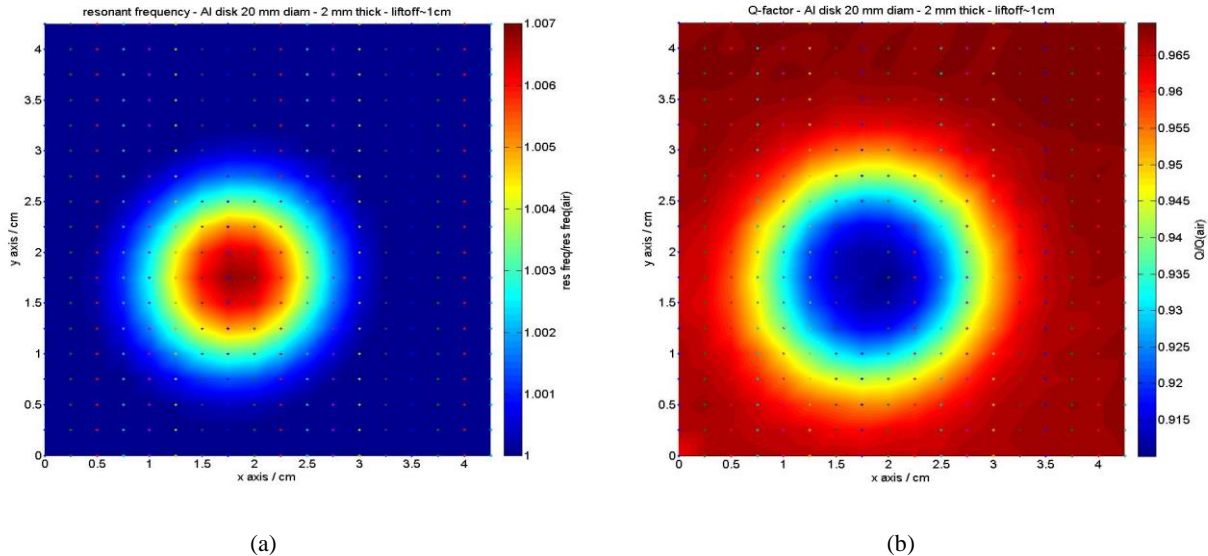


Figure 2. Images of a 2-cm-diameter 2-mm-thick unshielded Al disk; the images were obtained by means of position-resolved-measurements of the resonant frequency (a) and the Q-factor (b). In both cases, measurements were performed by using an LCR circuit with $L=(680\pm 10\%) \mu\text{H}$, $C=(1\pm 1\%) \mu\text{F}$ and $R=(4\pm 1\%) \text{M}\Omega$, at a lift-off equal to $l=(1.0\pm 0.1) \text{cm}$.

Not only do these images show the presence of the sample, they also reproduce its shape and size. A quantitative analysis aimed at determining the diameter of the imaged disk is reported in a previous work¹⁵. This showed good agreement between the diameter of the imaged disk estimated from the image and the actual sample's diameter. Images similar to the ones reported in Figure 2 were obtained with all the other metals considered for this study, including low-conductivity Mn, with which the lower amount of eddy currents compared to the one obtained with higher-conductivity samples was compensated for by decreasing the system capacitance, thus producing a higher shift in the resonant frequency measured in the presence of the material.

3.2 LCR circuit optimization

Results of the LCR circuit optimization study (see Sec. 2.2) are summarized here. Figures 3-4 show the relative changes in resonant frequency and Q-factor obtained by means of formulae (4) and (5), plotted against the Q-factor measured for each of the eight LCR circuits listed in Table 1. These figures show that both Δf_r and ΔQ increase when the circuit's Q-factor is increased. Choice of an appropriate combination of L, C and R provides a maximum change in the measured quantities which is nearly equal to 6.7% for the Q-factor and is about 0.7% for the resonant frequency.

An interesting observation can be made by looking at Figure 4: the Q-factor change becomes smaller for Q-factor circuits having values of $Q > 16$. This behavior is less pronounced when resonant frequency change is taken into account (Figure 3). The Q-factor trend shows that increasing Q up to values higher than 16 is not necessary and satisfactory change in the measured quantity can be obtained for $9.5 < Q < 16$.

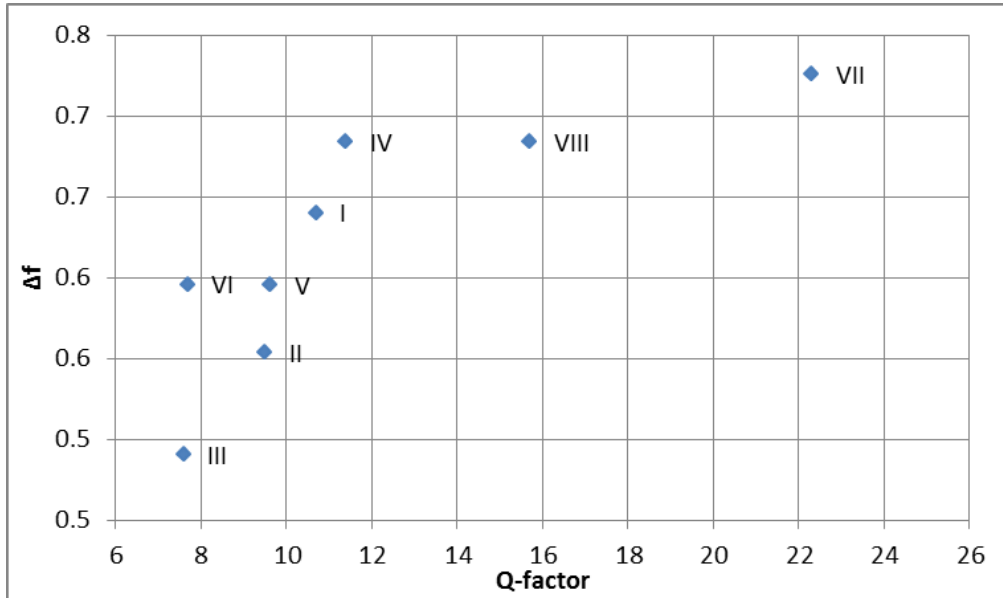


Figure 3. Relative change of resonant frequency (formula 4) produced by a $25 \times 25 \times 1 \text{ mm}^3$ Al sample for the eight LCR circuits listed in Table 1, having values of Q-factor going from 7.6 to 22.3.

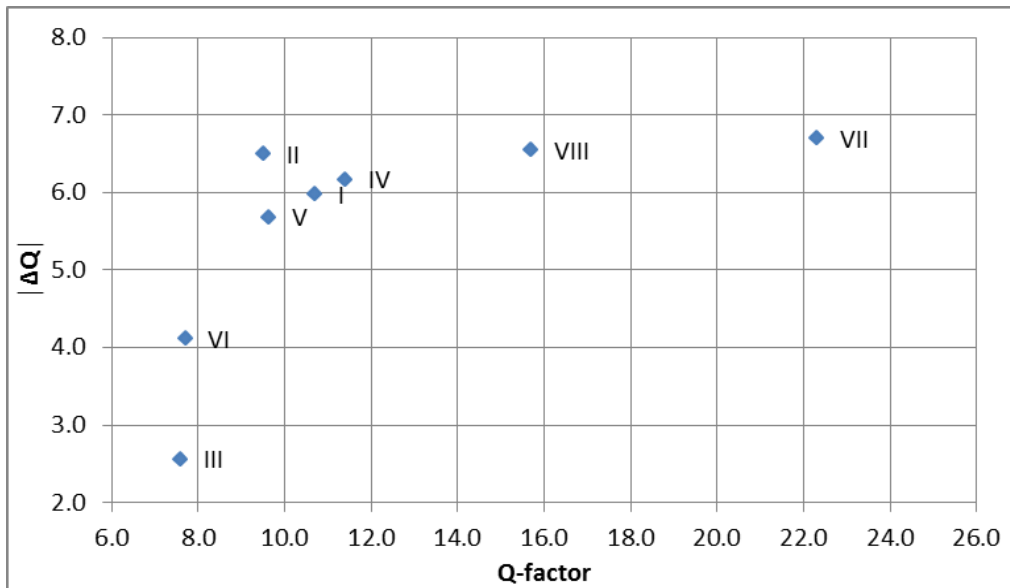


Figure 4. Relative change of Q-factor (absolute value of ΔQ expressed by formula 5) produced by a $25 \times 25 \times 1 \text{ mm}^3$ Al sample for the eight LCR circuits listed in Table 1, having values of Q-factor going from 7.6 to 22.3.

3.3 2D imaging of shielded conductive samples

Figure 5 shows 2D plots of a 6-cm-diameter 2-mm-thick Al disk shielded behind a 1.5-mm-thick Al sheet. Images were obtained by means of position-resolved-measurements of the resonant frequency (a) and the Q-factor (b). These results validate our proof-of-principle technique for 2D imaging of concealed metallic samples.

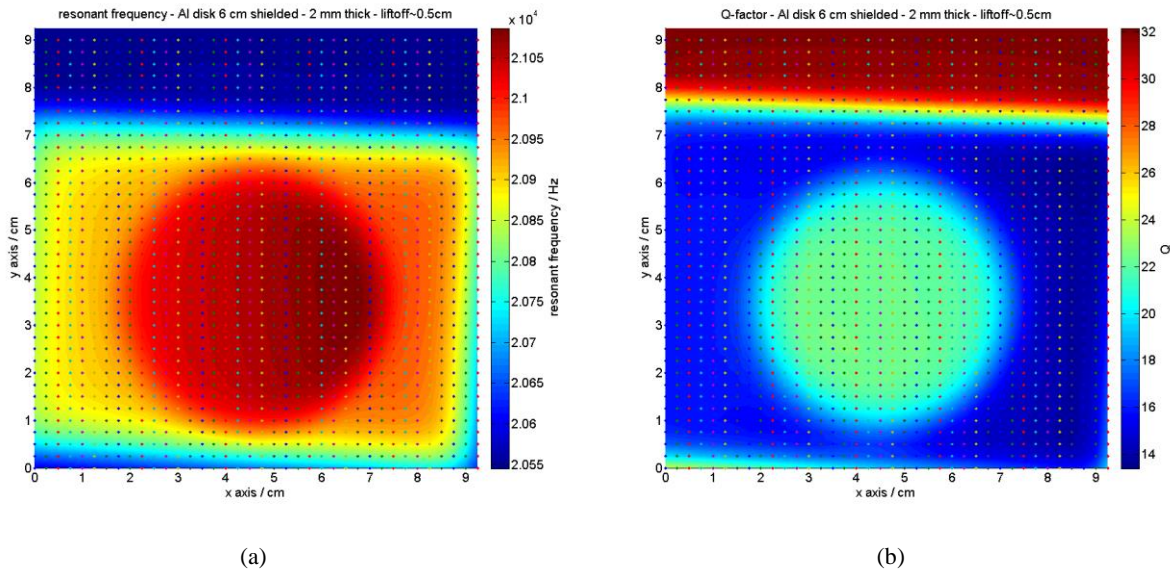


Figure 5. Images representing a 6-cm-diameter 2-mm-thick Al disk shielded by a 1.5-mm-thick Al sheet are shown in this figure. The images were obtained by means of position-resolved-measurements of the resonant frequency (a) and the Q-factor (b). In both cases, measurements were performed by using an LCR circuit with $L=(680\pm 10\%) \mu\text{H}$, $C=(0.1\pm 1.0\%) \mu\text{F}$ and $R=(10\pm 1\%) \text{K}\Omega$ at a lift-off equal to $l=(0.5\pm 0.1) \text{cm}$.

4. CONCLUSIONS

This work reported on preliminary results obtained with a novel EII system identified as a possible solution to the challenge of 2D imaging of concealed metallic objects. The investigations are particularly relevant in the field of national security, where the constant threat represented by traffic of illicit materials requires sensitive and reliable imaging and classification techniques to be developed. This system is an interesting candidate for 2D imaging of conductive samples hidden by conductive barriers, overcoming limitations of currently employed X-ray-based detection methods, which are not able to penetrate through metallic materials normally employed for shielding purposes. Results of our proof-of-principle method demonstrate the suitability of the proposed system to both detection and imaging of concealed metallic objects. In particular, samples covering a wide range of conductivities (0.54 to 59.77MSm^{-1}), hidden behind 1.5-mm-thick Al shields, were successfully revealed, and their shape and size were accurately reproduced. Our findings represent a step forward towards recognizing the presence of potentially hazardous or prohibited materials for security applications.

REFERENCES

- [1] Griffiths, H., "Magnetic induction tomography: a measuring system for biological tissues," *Meas. Sci. Technol.* 12, 1126-1131 (2001).
- [2] Zolgharni, M., Griffiths, H. and Ledger, P.D., "Frequency-difference MIT imaging of cerebral haemorrhage with a hemispherical coil array: numerical modelling," *Physiol. Meas.* 31, S111-S125 (2010).
- [3] Peyton, A.J., Yu, Z.Z., Lyon, G., Al-Zeibak, S., Ferreira, J., Velez, J., Linhares, F., Borges, A.R., Xiong, H.L., Saunders, N.H. and Beck, M.S., "An overview of electromagnetic inductance tomography: description of three different systems," *Meas. Sci. Technol.* 7, 261-271 (1996).
- [4] Ma, L., Wei, H-Y. and Soleimani, M., "Planar magnetic induction tomography for 3D near subsurface imaging," *Prog. Electromagn. Res.* 138, 65-82 (2013).
- [5] Soleimani, M., "Simultaneous reconstruction of permeability and conductivity in magnetic induction tomography," *J. of Electromagn. Waves and Appl.* 23, 785 (2009).
- [6] Higson, S. R., Drake, P., Stamp, D. W., Peyton, A., Binns, R., Lyons, A. and Lionheart, W., "Development of a sensor for visualization of steel flow in the continuous casting nozzle," *Revue de Metallurgie-Cahiers d'Informations Techniques* 100, 629-632 (2003).
- [7] Gaydecki, P., Quek, S., Miller, G., Fernandes, B.T. and Zaid, M.A.M., "Design and evaluation of an inductive Q-detection sensor incorporating digital signal processing for imaging of steel reinforcing bars in concrete," *Meas. Sci. Technol.* 13, 1327-1335 (2002).
- [8] Wei, H.Y. and Soleimani, M., "A magnetic induction tomography system for prospective industrial processing applications," *Chinese J. Chem. Eng.* 20(2), 406-410 (2012).
- [9] Darrer, B. J., Watson, J. C., Bartlett, P. and Renzoni, F., "Magnetic Imaging: a New Tool for UK National Nuclear Security," *Sci. Rep.* 5 7944, 1-6 (2015).
- [10] Darrer, B. J., Watson, J. C., Bartlett, P. and Renzoni, F., "Electromagnetic imaging through thick metallic enclosures," *AIP Advances* 5, 087143, 1-8 (2015); <http://dx.doi.org/10.1063/1.4928864>.
- [11] Deans, C., Marmugi, L., Hussain, S. and Renzoni, F., "Electromagnetic induction imaging with a radio-frequency atomic magnetometer," *Appl. Phys. Lett.* 108, 103503, 1-5 (2016); <http://dx.doi.org/10.1063/1.4943659>.
- [12] Marmugi, L. and Renzoni, F., "Optical magnetic induction tomography of the heart," Submitted to *Scientific Reports*.
- [13] Du, L., Zhu, X., Han Y., Zhao L. and Zhe J., "Improving sensitivity of an inductive pulse sensor for detection of metal wear debris in lubricants using parallel LC resonance method," *Meas. Sci. Technol.* 24(7), 1-10 (2013).
- [14] Du, L. and Zhe J., "Parallel sensing of metallic wear debris in lubricants using undersampling data processing," *Tribology International* 53, 28-34 (2012).
- [15] Guilizzoni, R., Watson, J. C., Bartlett, P. and Renzoni, F., "Imaging by electromagnetic induction with resonant circuits," *Proc. SPIE* 9481, *Image Sensing Technologies: Materials, Devices, Systems, and Applications II*, 94810Q (May 13, 2015); <http://dx.doi.org/10.1117/12.2183180>.
- [16] Weast, R.C., [Handbook of Chemistry and Physics], Boca Raton: CRC Press, 60th edition, Florida, E85-F172 (1979-1980).
- [17] Canny, J.F., "A computational approach to edge detection," *IEEE Transactions on pattern analysis and machine intelligence* 8(6), 679-698 (1986).